Molecular Biology of the Cell
Vol. 18, 4377–4386, November 2007

Rab27b Is Expressed in a Wide Range of Exocytic Cells and Involved in the Delivery of Secretory Granules Near the Plasma Membrane

Hiroshi Gomi,* Kenichi Mori,* Shigeyoshi Itohara,† and Tetsuro Izumi*

*Laboratory of Molecular Endocrinology and Metabolism, Institute for Molecular and Cellular Regulation, Gunma University, Maebashi 371-8512, Japan; and †Laboratory for Behavioral Genetics, Brain Science Institute, Institute of Physical and Chemical Research, Wako 351-0198, Japan

Submitted May 4, 2007; Revised June 29, 2007; Accepted August 17, 2007
Monitoring Editor: Francis Barr

Rab proteins regulate multiple, complex processes of membrane traffic. Among these proteins, Rab27a has been shown to function specifically in regulated exocytic pathways. However, the roles of Rab27b, another Rab27 subfamily member, have not been well characterized. We disrupted the Rab27b gene in mice. The targeting vector was designed to insert *LacZ* downstream of the initiation codon of the Rab27b gene so that the authentic promoter should drive this reporter gene. A comprehensive analysis of Rab27b expression using this mouse strain indicated that it is widely expressed not only in canonical secretory cells, but also in neurons and cells involved in surface protection and mechanical extension. To evaluate the function in pituitary endocrine cells where the isoform Rab27a is coexpressed, we generated Rab27a/Rab27b double knockout mice by crossing Rab27b knockout mice with Rab27a-mutated *ashen* mice. The polarized distribution of secretory granules close to the plasma membrane was markedly impaired in the pituitary of double knockout mice, indicating that the Rab27 subfamily is involved in the delivery of granules near the exocytic site. In conjunction with a phenotype having a pituitary devoid of the Rab27 effector granuphilin, we discuss the relationship between the residence and the releasable pool of granules.

INTRODUCTION

The Rab GTPases are composed of more than 60 members in mammals. Each Rab has distinct subcellular localizations and regulates a specific step of intracellular vesicle trafficking by binding with its effector protein (Grosshans *et al.*, 2006). Rab27a has recently been recognized to function in the exocytic pathways of various secretory vesicles based on the following findings. First, loss-of-function mutations of the Rab27a gene cause partial cutaneous albinism and immunodeficiency in human patients having Griscelli syndrome (Ménasché *et al.*, 2000) and in the coat-color mutant mouse *ashen* (Wilson *et al.*, 2000). These symptoms reflect defects in the transfer of melanosomes from melanocytes to keratinocytes and in the exocytosis of lytic granules in cytotoxic T lymphocytes, respectively. Second, Rab27a associates with classical secretory granules (Yi *et al.*, 2002), as well as with lysosome-related organelles such as melanosomes (Bahadoran *et al.*, 2001; Hume *et al.*, 2001) and lytic granules (Haddad *et al.*, 2001; Stinchcombe *et al.*, 2001), and plays versatile roles in the exocytosis of these organelles by utilizing multiple effector proteins (Izumi *et al.*, 2003; Fukuda, 2005). Third, the construction of a transgenic mouse that expresses an enhanced green fluorescent protein (EGFP)-Rab27a fusion protein under the control of endogenous Rab27a promoter reveals that the fusion protein is widely expressed in specialized secretory cells, including exocrine, endocrine, ovarian, and hematopoietic cells (Tolmachova *et al.*, 2004). Taken together, these findings suggest that Rab27a functions in a broad range of exocytic pathways.

Unlike Rab27a, the Rab27b isoform of the Rab27 subfamily has not been well characterized, and no human disease or animal strain with mutations in the Rab27b gene has been identified. Although Rab27b is known to localize on pituitary endocrine granules (Zhao *et al.*, 2002), dense and α-granules in platelets (Barral *et al.*, 2002) and megakaryocytes (Tiwari *et al.*, 2003), urothelial fusiform vesicles (Chen *et al.*, 2003), and parotid and pancreatic acinar granules (Chen *et al.*, 2004; Imai *et al.*, 2004), its expression has been thought to be more restricted than that of Rab27a. In the present study, we constructed a knockin mouse, which lacks the Rab27b gene and instead expresses *LacZ* under the control of authentic Rab27b promoter. By analyzing the *LacZ* expression, we thoroughly characterized the Rab27b expression in specific cell types of various tissues. The result indicated that Rab27b is widely expressed not only in classical secretory cells but also in those providing surface membrane in response to mechanical stress. To evaluate the whole function of the Rab27 subfamily in vivo, we generated Rab27a/Rab27b double knockout mice by crossing the Rab27b-deficient mice with *ashen* mice. Morphological and functional analyses of pituitary cells demonstrated that the Rab27 subfamily plays a critical role in the localization of secretory granules in the cell periphery close to the plasma membrane, but not in the release process itself.

This article was published online ahead of print in *MBC in Press* (http://www.molbiolcell.org/cgi/doi/10.1091/mbc.E07–05–0409) on August 29, 2007.

Address correspondence to: Tetsuro Izumi (tizumi@showa.gunma-u.ac.jp).

MATERIALS AND METHODS

Generation of Rab27b-deficient Mice and Doubly Mutated Mice Lacking Rab27a and Rab27b

The genomic DNA clones of mouse *Rab27b* were isolated from a 129/Sv BAC genomic library by screening with a mouse cDNA fragment (Zhao *et al.*, 2002). The targeting vector was constructed with a 4.7-kb PstI-BsmAI fragment that spans from intron 1 to exon 2 as a 5′ homologous region, a 6.5-kb ScaI-NheI fragment from intron 2 to intron 4 as a 3′ homologous region, a 2.1-kb floxed *pgk-neo* fragment in which a *neo* gene under the control of *pgk* promoter (a gift from M. A. Rudnicki, The Ottawa Health Research Institute, Ottawa, Canada) is flanked by two *loxP* sequences, and a 1.4-kb *DTA* gene cassette derived from p*MC1DTA-pA* (a gift from T. Yagi, Osaka University, Suita, Japan; Yanagawa *et al.*, 1999). The targeting vector p5′PB-*NLacZ-pgk-neo*-3′SN-*DTA* was constructed as follows. A 4.7-kb 5′ homologous DNA fragment was inserted into a PstI-HindIII site of pBl*NLacZ* vector (a gift from K. Yamamura, Kumamoto University, Kumamoto, Japan), resulting in p5′PB-*NLacZ*. Separately, a 1.4-kb *DTA* gene cassette was blunt-ligated into an ApaI site of the p*pgk-neo* vector, resulting in p*pgk-neo-DTA*. A 6.5-kb 3′ homologous ScaI-NheI fragment was cloned into a XhoI site of the p*pgk-neo-DTA* vector, resulting in p*pgk-neo*-3′SN-*DTA*. Finally, a 5′PB-*NLacZ* homologous fragment was excised as one fragment from p5′PB-*NLacZ* and ligated into a NotI-blunted-SacII site of p*pgk-neo*-3′SN-*DTA* to generate p5′PB-*NLacZ-Neo*-3′SN-*DTA*. The targeting vector was electroporated into embryonic day (E) 14 embryonic stem (ES) cells (a gift from M. Hooper, Western General Hospital, Edinburgh, United Kingdom), and G418-resistant clones were selected, as described previously (Gomi *et al.*, 1995). Homologous recombinants were isolated by Southern blot hybridization, using a GeneScreen Plus Hybridization Transfer Membrane (Perkin Elmer Life and Analytical Sciences, Wellesley, MA) and an alkaline phosphatase–labeled (AlkPhos Direct, GE Healthcare Bio-Science, Piscataway, NJ) external probe. The ES cell clones containing the targeting event were microinjected into C57BL/6J blastocysts to generate chimeric mice. The mice heterozygous for the targeted allele (*Rab27b*$^{+/-}$) were obtained by crossing the male chimeras with female C3H/He mice. Mutant lines were maintained as heterozygotes by backcrossing with C3H/He mice. Genotype analysis was done by Southern hybridization and/or PCR. The primers designed for the exon 2 region of *Rab27b* and *NLacZ* were as follows: *Rab27b/Fow*, 5′-GCATGCAGAGTGAATCAACT-3′; *Rab27b/Rev*, 5′-CAAGAGATAGCGTCACTCAAC-3′; and *NLacZ/Rev*, 5′-TGTGAGCGAGTAACAACCCG-3′.

The *Rab27b*$^{-/-}$ mice were crossed with Rab27a natural mutant mice, *ashen* (Wilson *et al.*, 2000; Kasai *et al.*, 2005), to obtain *Rab27a*$^{+/ash}$*Rab27b*$^{+/-}$ doubly heterozygous mice. Intercrossing of doubly heterozygous mice was performed to obtain doubly mutated mice lacking Rab27a and Rab27b (*Rab27a*$^{ash/ash}$-*Rab27b*$^{-/-}$). For genotyping of the *ashen* mutation in *Rab27a*$^{+/ash}$ mice, the genomic region that contains the splice donor site located downstream of exon 4 of *Rab27a* was amplified by PCR using the following primers: *Rab27a/Fow*, 5′-TGTGCCCTAGGTTTCGTAGCTTAACC-3′; and *Rab27a/Rev*, 5′-GTAGCCTCGACACTGAGCTGTTTCC-3′. An RsaI-sensitive internal digestion of the wild-type *Rab27a* fragment produced shorter fragments that were distinguishable from an *Rsa*I-insensitive *ashen* fragment. The mice had free access to water and standard laboratory chow (CE-2, CLEA Japan, Tokyo, Japan) in an air-conditioned room with a 12-h light/dark cycle. All animal experiments were done according to the guidelines of the Animal Care and Experimentation Committee, Gunma University.

LacZ Staining

Mice anesthetized with sodium pentobarbital (100 μg/g body weight) were fixed with 50 ml of 3.8% formaldehyde in 0.1 M sodium phosphate buffer (PB), pH 7.4, via cardiac perfusion at 4°C for 10 min after washing out the blood with 10 ml of physiological saline perfusion. Fixed samples taken from various organs were cut into small thin pieces ($<2 \times 2$ mm) and washed several times in ice-cold PB. Fixed brain tissue was coronally sliced on a Microslicer DTK-1000 (Dosaka EM, Kyoto, Japan) to a 400-μm thickness in ice-cold PB. The washed tissue specimens were stained in PB containing 5 mM $K_3Fe(CN)_6$, 5 mM $K_4Fe(CN)_6$, 2 mM $MgCl_2$, and 1 mg/ml 5-bromo-4-chloro-3-indolyl-β-D-galactoside (X-gal) for 4–6 h at 37°C. After *LacZ* staining, the tissue specimens were postfixed with the same fixative. Some of them were then immersed in 30% sucrose solution overnight at 4°C, embedded in Tissue-Tek OCT compound (Sakura Finetek, Torrance, CA), and processed for cryosection (5 or 25 μm) on a cryotome (Leica, Nussloch, Germany). Cryosections were mounted on 3-aminopropyl-triethoxysilane–coated slide glass and counterstained with 1% safranine-O. Image acquisition was done using an MZ12 stereoscopic microscope (Leica) for the tissue specimens or a BX50 microscope equipped with a DP-70 charge-coupled device camera (Olympus, Tokyo, Japan) for the sections.

Immunohistochemistry

Mice were anesthetized and then fixed with 4% paraformaldehyde in PB via cardiac perfusion at 4°C for 20 min. The pituitary was removed, postfixed with the same fixative overnight at 4°C, equilibrated in 30% sucrose, and then frozen in OCT compound. For immunohistochemistry of the bone marrow aspirates, bladder, and pituitary, sections (5 or 15 μm) were prepared on a cryotome. The sections were washed with phosphate-buffered saline (PBS; 137 mM NaCl, 2.68 mM KCl, 8.10 mM Na_2HPO_4, 1.47 mM KH_2PO_4, pH 7.3) and permealized with PBS containing 0.1% Triton X-100 for 15 min. Nonspecific reactions were blocked by incubation with PBS containing 5% normal goat serum and 50 mM NH_4Cl for 30 min at room temperature. Subsequently, the sections were reacted with mouse anti-β-galactosidase mAb (1:2000 dilution; Promega, Madison, WI) or affinity-purified rabbit anti-Rab27b antibody (1:1000–10,000 dilution; Zhao *et al.*, 2002) overnight at 4°C. After repeated washes with PBS, the sections were reacted with goat Alexa 546– or 488–conjugated anti-rabbit IgG antibody or goat Alexa 488–conjugated anti-mouse IgG antibody (1:1500–3000 dilution, Molecular Probes/Invitrogen, Carlsbad, CA). Images were acquired with a BX50 microscope equipped with an epifluorescence attachment (Olympus) and a SenSys charge-coupled device camera (Photometrics, Tucson, AZ).

Immunoblot Analysis

After removal from the cranium, the pituitary was put in PBS solution and separated into anterior and intermediate lobes at the vestigial cleft of Rathke's pouch with a needle edge under stereoscopy. Each lobe was frozen with liquid nitrogen and stored at −80°C. Frozen tissues were thawed and homogenized with lysis buffer containing 20 mM Tris, pH 7.5, 150 mM NaCl, 2.5 mM $MgCl_2$, 1 mM EGTA, 1.0% Triton X-100, and 1 × protease inhibitor cocktail (Complete mini, Roche Diagnostics, Mannheim, Germany). The homogenates were kept on ice for 20 min and then spun at 20,000 × *g* for 10 min. The supernatant was collected, and the protein concentration was determined using a Coomassie brilliant blue protein assay reagent (Nacalai tesque, Kyoto, Japan). The extracted protein was subjected to SDS-PAGE and transferred to an Immobilon-P transfer membrane (Millipore, Billerica, MA). After blocking with 5% skimmed milk in Tris-buffered saline supplemented with 0.05% Tween 20 for 1 h, the membrane was incubated with primary and secondary antibodies at the following dilutions: rabbit anti-Rab27b antibody (1:1000); rabbit anti-granuphilin antibody αGrp-N (1:2000; Yi *et al.*, 2002); monoclonal anti-HPC-1/syntaxin-1a/1b (1:3000) and anti-α-tubulin (1:3000) antibodies (Sigma Aldrich, St. Louis, MO); monoclonal anti-Rab3a (1:1000), anti-Rab27a (1:1000), and anti-Munc18–1 (1:300) antibodies (BD Biosciences, San Jose, CA); and horseradish peroxidase–labeled goat anti-rabbit or anti-mouse IgG (1:5000; Jackson ImmunoResearch Laboratory, West Grove, PA). Antibody detection was accomplished using enhanced chemiluminescent Western blotting detection reagents (GE Healthcare Bio-Science).

Glutathione *S*-transferase (GST)-fused mouse recombinant Rab27a and Rab27b proteins were bacterially expressed and affinity-purified with glutathione-Sepharose 4B (GE Healthcare BioScience), as previously described (Yi *et al.*, 2002; Zhao *et al.*, 2002). The concentration of purified GST-fused proteins was determined by Coomassie brilliant blue staining in polyacrylamide gel by comparison with the reference concentration of bovine serum albumin. To estimate the expression levels of Rab27a and Rab27b in the mouse pituitary, the comparable immunoreactivities of the endogenous proteins extracted from pituitary tissue to the recombinant proteins were examined by immunoblot analysis using anti-Rab27a and anti-Rab27b antibodies.

Electron Microscopy

The excised pituitary was fixed by an immersion shaking with 2% paraformaldehyde/2.5% glutaraldehyde/0.2% picric acid in 0.1 M cacodylate buffer (pH 7.4) for 5 h. The sample was then cut in the medianus and postfixed with 2% osmium tetroxide in 0.1 M cacodylate buffer at 4°C for 1.5 h. The tissue blocks were dehydrated, infiltrated, and embedded in plastic resin. Ultrathin (90 nm) sections were cut on an Ultracut E ultramicrotome (Reichert-Jung, Vienna, Austria), stained with uranyl acetate and lead citrate, and subjected to analysis with a JEM 1010 transmission electron microscope (JEOL, Tokyo, Japan) at an acceleration voltage at 80 kV. The electron microscopic pictures (magnifications at 5000× and 30,000×) were scanned at 720 dpi with an ES-2200 image scanner (Epson, Suwa, Japan) to acquire the digital image. For morphometry of the granule distribution in corticotrophs, the images (5000×) were analyzed by Particle Analysis software (O'Hara, Tokyo, Japan) to measure the distance from each granule center to the nearest plasma membrane. Cell and granule sizes were measured by Image J 1.31 software, as described previously (Gomi *et al.*, 2005).

Perifusion Secretion Assays in Isolated Pituitary

The pituitaries were aseptically removed from anesthetized mice and divided into anterior and intermediate-posterior lobes in RPMI 1640 medium supplemented with 10% fetal calf serum. The anterior lobe was preincubated with oxygen-saturated Krebs-Ringer buffer (KRB; 10 mM HEPES, pH 7.4, 118.4 mM NaCl, 4.7 mM KCl, 1.9 mM $CaCl_2$, 1.3 mM $MgSO_4$, 1.2 mM KH_2PO_4, 25 mM $NaHCO_3$, 0.1% bovine serum albumin, 11 mM glucose) for 3 h. One tissue specimen was placed at the bottom of a 1-ml syringe that had been cut to a volume of 400 μl and plugged with cotton. The tissue was perifused with KRB at a constant flow rate of 500 μl/min for 40 min. After preincubation, the tissue was stimulated with 10 nM corticotropin-releasing factor (CRF; Calbiochem/Merck Bioscience, Darmstadt, Germany) for 15 min and then with 60 mM KCl for 10 min. All the preincubation and perifusate solutions were

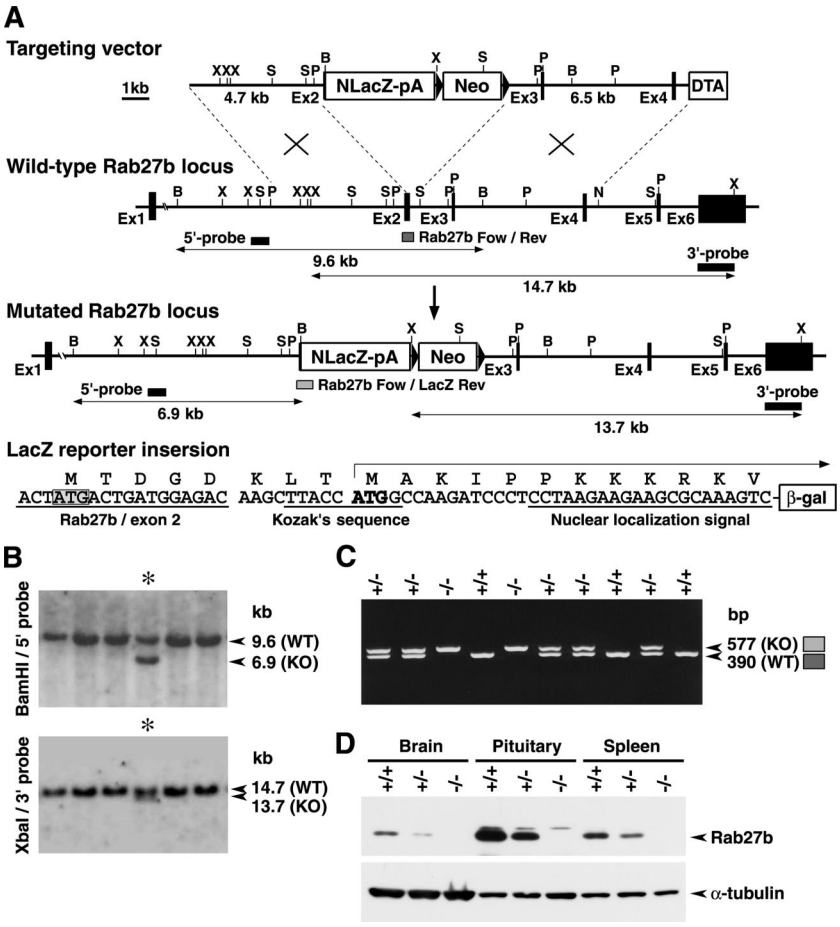

Figure 1. Generation of *Rab27b* knockout mice. (A) Targeted disruption of the Rab27b gene on mouse chromosome 18 by insertion of *NLacZ* (*LacZ* gene with a nuclear localization signal). The targeting vector contains a neomycin resistance gene driven by the *pgk* promoter (Neo) and a diphtheria toxin A-fragment gene driven by the *MC1* promoter (DTA) as positive and negative selection markers, respectively. Exon structures are vertically lined and partially shown from the first (Ex1) to the sixth exon (Ex6). Homologous recombination results in replacement of the genomic region from the second exon with *NlacZ-pA-Neo*. The *LacZ* reporter gene with a Kozak's sequence and a nuclear localization signal is inserted five amino acids downstream of the initiation codon of the *Rab27b* second exon. B, BamHI; N, NheI; P, PstI; S, ScaI; X, XbaI restriction sites. (B) Genomic Southern hybridization analysis of the neomycin resistant ES cell clones. The locations of the 5′ external probe and the 3′ external probe are shown with horizontal closed boxes in A. The 5′ probe hybridizes to *Bam*HI fragments of 9.6 and 6.9 kb from wild-type (*Rab27b*$^{+}$; WT) and mutant (*Rab27b*$^{-}$; KO) alleles, respectively. Similarly, the 3′ probe hybridizes to *Xba*I fragments of 14.7 and 13.7 kb from the WT and KO alleles, respectively. Asterisks indicate a homologously recombinant ES cell clone. (C) PCR-genotyping of F2 progenies from a cross of F1 heterozygotes. Positions of PCR-amplified DNA fragments in genotyping from the wild-type allele (*Rab27b-Fow/Rev*) and mutated allele (*Rab27b-For/LacZ-Rev*) are shown as dark and light-gray boxes, respectively, in A. PCR with *Rab27b-Fow*, *Rab27b-Rev*, and *LacZ-Rev* mixed primers produced 577 base pairs (KO), 390 base pairs (WT), and both fragments (hetero-type). −/−, homozygous *Rab27b*$^{-/-}$; +/−, heterozygous *Rab27b*$^{+/-}$; +/+, wild-type *Rab27b*$^{+/+}$. (D) Immunoblot analysis of Rab27b knockout mice. Twenty micrograms of proteins from brain, pituitary, and spleen tissues were electrophoresed for immunoblotting with anti-Rab27b and α-tubulin antibodies.

equilibrated with 95% O_2 and 5% CO_2 and maintained at 37°C. After perfusion, the tissues were extracted in an acid-ethanol solution (70% ethanol and 0.18 M HCl), and adrenocorticotropic hormone (ACTH) was measured using an ACTH immunoradiometric assay kit (Mitsubishi Kagaku Iatron, Tokyo, Japan).

RESULTS

Generation of Rab27b Mutant Mice

To identify the cell types that express Rab27b in detail and to address the function of Rab27b in vivo, we disrupted *Rab27b* in mice using a gene-targeting technique. Rab27b mutant mice were generated by deletion of a genomic region from exon 2 to intron 2 in ES cells (Figure 1A). The promoterless *LacZ* gene with a nuclear localization signal was inserted so that β-galactosidase was expressed as a fusion protein to the amino-terminal 5-amino acid residues of Rab27b. After knockin by homologous recombination, *LacZ* was expected to be expressed under the authentic promoter activity of *Rab27b*. Homologous recombinants were identified by Southern hybridization of the genomic DNA (Figure 1B). PCR analysis of the tail DNA showed that the intercrosses between the heterozygotes (*Rab27b*$^{+/-}$) give rise to homozygotes (*Rab27b*$^{-/-}$), heterozygotes (*Rab27b*$^{+/-}$), and wild-type mice (*Rab27b*$^{+/+}$) at the frequency of 1:2:1 (Figure 1C). Immunoblot analysis showed that *Rab27b*$^{-/-}$ mice completely lacked Rab27b in the brain, pituitary, and spleen (Figure 1D), where Rab27b is normally expressed at high levels (Zhao *et al.*, 2002). Mutant mice showed normal development and were fertile, with no apparent abnormalities in general appearance or behavior.

Tissue and Cell Type–specific Expression of Rab27b

To determine whether the *LacZ* gene inserted in the *Rab27b* locus was expressed similarly as the endogenous *Rab27b*, we examined the correlation between the *LacZ* activity and the immunostaining signal with anti-Rab27b antibody in the tissues where Rab27b expression had previously been established. In the bone marrow aspirates of wild-type *Rab27b*$^{+/+}$ mice, the huge cells with large irregular and multilobular nuclei showed punctate immunostaining signals in the cytoplasm (Figure 2A), consistent with the previous finding that Rab27b localize on the dense and the α-granules in megakaryocytes (Tiwari *et al.*, 2003). These signals are specific because they were not seen in the megakaryocytes of *Rab27b*$^{-/-}$ mice (Figure 2C). Conversely, the *LacZ* staining revealed strong activity in the nuclei of the megakaryocytes from *Rab27b*$^{-/-}$ mice, but not those from *Rab27b*$^{+/+}$ mice (Figure 2, B and D). Similarly, in the urinary bladder, Rab27b was specifically expressed in the umbrella cells lining the surface of the transitional epithelium of *Rab27b*$^{+/+}$ mice, but not of *Rab27b*$^{-/-}$ mice (Figure 2, E and G). By contrast, *LacZ* was expressed in the nuclei of those cells from *Rab27b*$^{-/-}$ mice, but not from *Rab27b*$^{+/+}$ mice (Figure 2, F and H). Rab27b is associated with the fusiform vesicles in these cells

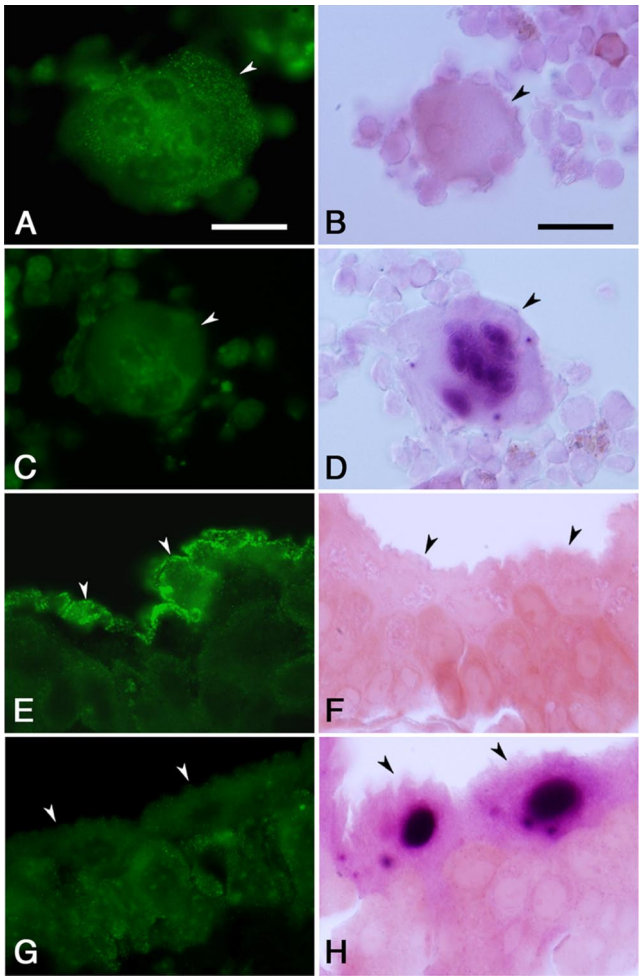

Figure 2. Comparison of expression pattern of Rab27b and *LacZ*-reporter gene activity. The megakaryocytes with multilobular nuclei (A–D) isolated from femoral bone marrow (arrowhead) and the umbrella cells (E–H) located on the inner surface of the urinary bladder (arrowheads) from *Rab27b*$^{+/+}$ (A, B, E, and F) and *Rab27b*$^{-/-}$ (C, D, G, and H) mice were analyzed by immunohistochemistry with anti-Rab27b antibody (left panels) or *LacZ* staining (right panels). After *LacZ* staining, tissues were cryosectioned (5-μm thick) and counterstained with safranine-O (red color). Bars, 20 μm.

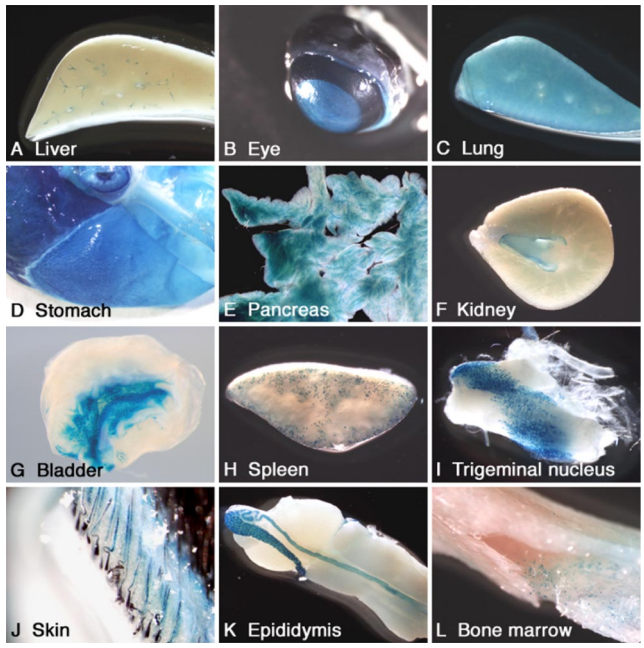

Figure 3. *LacZ* expression in peripheral tissues of *Rab27b*$^{+/-}$ mice. Blue-color staining of each tissue indicates *LacZ*-positive regions in macroview.

and is suggested to play a regulatory role in their delivery to the apical plasma membrane (Chen *et al.*, 2003). These findings indicate that *LacZ* expression in the mutant mice faithfully represents the endogenous expression of Rab27b.

In the organ level, *LacZ* expression was detected in the liver, eye, lung, stomach, pancreas, kidney, urinary bladder, and spleen (Figure 3, A–H). The expression pattern of *LacZ* correlated well with that of Rab27b, as previously determined by immunohistochemistry, immunoblot and Northern blot hybridization, and reverse transcription-PCR analyses (Ramalho *et al.*, 2001; Zhao *et al.*, 2002; Chen *et al.*, 2003, 2004). In addition, *LacZ* expression was also detected in the trigeminal nucleus, skin, epididymis, and bone marrow cells (Figure 3, I–L). In the CNS, *LacZ* activity was detected in neurons in various brain regions including the cerebral cortex, caudate-putamen, hippocampus, amygdala, thalamus, hypothalamus, midbrain, cerebellar deep nuclei, pontine nuclei (Figure 4), and spinal cord (data not shown). Consistent with our previous report (Zhao *et al.*, 2002), *LacZ* was expressed in the pituitary tissues, which is described in detail later.

We then analyzed *LacZ* expression in the section level. Because the staining signal was located almost exclusively in the cell nucleus, we could sensitively identify *Rab27b* expression with single-cell resolution. In the gastrointestinal tract, *LacZ* was highly expressed in the mucous-secreting cells located in the luminal surface and the basal side of the gastric glands (Figure 5A). In addition, acid-secreting parietal cells with a characteristic fried egg shape showed weaker expression. In the esophagus, *LacZ* was expressed in a thick protective stratified squamous epithelium (Figure

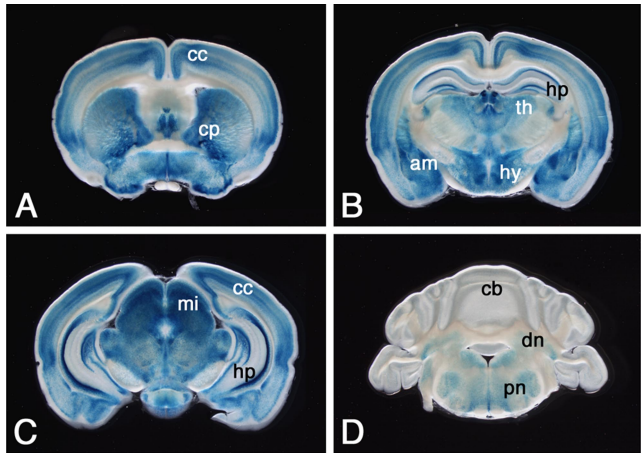

Figure 4. *LacZ* expression in brain tissue of *Rab27b*$^{+/-}$ mice. The images from A to D are arranged in order of coronal brain slices (400-μm thickness) from the rostral to the caudal. cc, cerebral cortex; cp, caudate-putamen; hp, hippocampus; am, amygdala; th, thalamus; hy, hypothalamus; mi, midbrain; cb, cerebellar cortex; dn, cerebellar deep nuclei; pn, pontine nuclei.

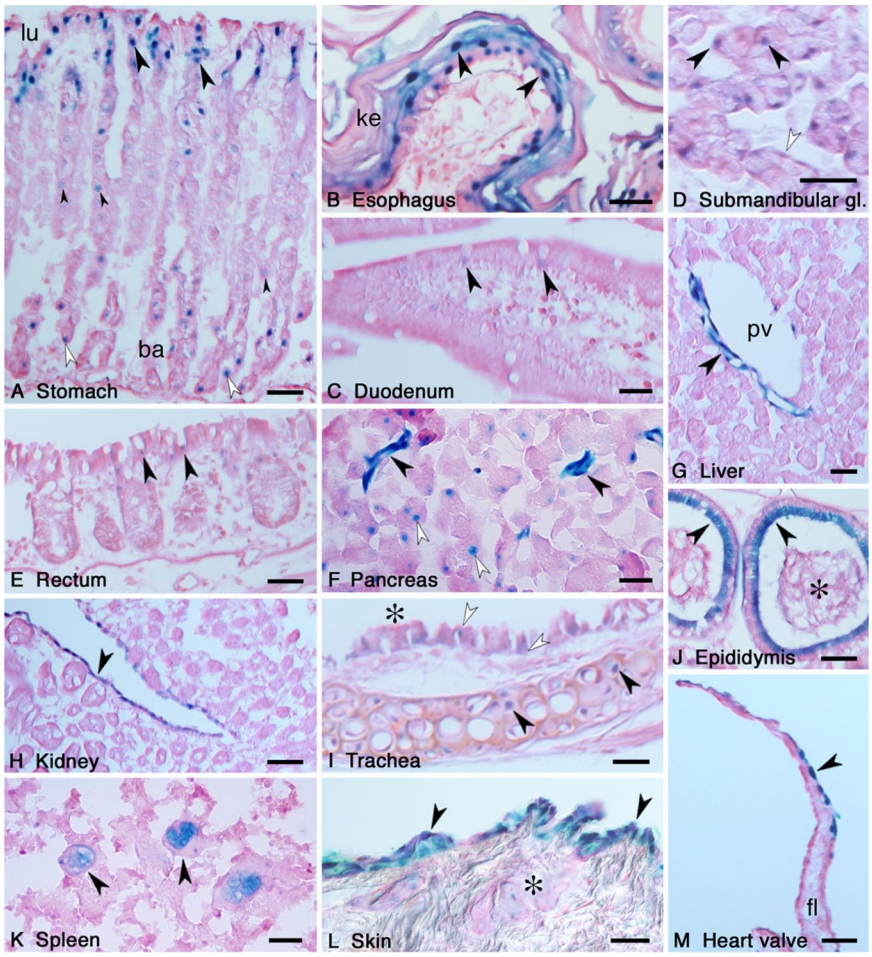

Figure 5. Analysis of *LacZ* expression in the section level. After *LacZ* staining, tissues were postfixed, and the cryosections were counterstained with safranine-O (red color). (A) Longitudinal sectioning of the stomach. *LacZ* was expressed in the tall columnar mucous-secreting cells of the luminal surface (lu) of the stomach (arrowheads). In the basal side (ba) of the gastric glands, neck mucous cells expressed *LacZ* (open arrowheads). Acid-secreting parietal cells slightly expressed *LacZ* (small arrowheads). (B) In the surface of the esophagus, the stratified squamous epithelium cells expressed *LacZ* (arrowheads). The surface-most layer of the epithelium was keratinized (ke). (C) Longitudinal sectioning of the duodenum. *LacZ* was expressed in the goblet cells of the mucosal villi (arrowheads). (D) In the submandibular salivary glands, both the serous (arrowheads) and mucous secretory cells (open arrowheads) expressed *LacZ*. (E) *LacZ* was expressed in the goblet cells of the rectum (arrowheads). (F) In the exocrine pancreas, the duct cells (arrowheads) showed stronger *LacZ* expression than did the acinar cells (open arrowheads). (G) In the liver, possible endothelial cells at terminal branches of the hepatic artery expressed *LacZ* (arrowhead). pv, portal vein in the portal tract. (H) In the kidney, the transitional epithelium of the renal pelvis expressed *LacZ* (arrowhead). (I) *LacZ* expression of hyaline cartilage cells (arrowheads) in the trachea. Goblet cells (open arrowheads) located in the ciliated respiratory epithelium (asterisk) also expressed *LacZ*. (J) *LacZ* was expressed in the pseudostratified tall columnar epithelia of the epididymis (arrowheads). An asterisk indicates the spermatozoa stored in the epididymal duct. (K) In the spleen, large nuclear macrophages expressed *LacZ* (arrowheads). (L) A section of the skin, after shaving the hair and reducing the surface cornified layer, showed *LacZ* expression in the epidermal keratinocytes (arrowheads) and sebaceous gland (asterisk). (M) Endothelial cells of the heart valve expressed *LacZ* (arrowhead). fl, fibrous lamina. Bars, 20 μm.

5B). The staining was strong in large polygonal cells of the intermediate layer and in the cuboidal cells of the basal layer, whereas it was at a remnant level in the flattened surface layer formed by keratinized cells. Sections of small intestine (duodenum) and large intestine (rectum) revealed slight but clear expression of *LacZ* in goblet cells located in the mucosal villi of the epithelial layer (Figure 5, C and E). In the submandibular salivary glands, mixed sero-mucous secretory unit cells exhibited *LacZ* activity (Figure 5D). A higher expression was observed in the serous aciner cells that had round-shaped nuclei and densely counterstained cytoplasm containing zymogen granules, whereas a moderate expression was detected in the mucous acinar cells that had flat-shaped nuclei and poorly counterstained cytoplasm containing mucigen granules. Consistent with the previous finding of Rab27b localization on zymogen granules (Chen *et al.*, 2004), overall *LacZ* activity was detected in the exocrine pancreas (Figure 3E). On the section level, however, pancreatic duct cells showed a more intense activity than exocrine acinar cells (Figure 5F). In the liver, *LacZ* expression was observed in the tubular structures around the portal tract (Figure 5G). These were considered to be endothelial cells at the terminal branches of the hepatic artery based on their morphological characteristics of being in thick-walled, small-diameter vessels with flat, elongated nuclei. The simple columnar epithelium of the gall bladder also exhibited *LacZ* expression (data not shown).

In the kidney, *LacZ* was expressed exclusively in the transitional epithelium of the renal pelvis, but not in the renal parenchyma (Figure 5H). The renal pelvis is a funnel-shaped structure and represents the dilated proximal part of the ureter. The transitional epithelium lining the lumen of the ureter also expressed *LacZ* (data not shown).

In the respiratory tract, the tracheal section exhibited *LacZ* expression in two different types of cells: the hyaline cartilage cells and goblet cells in the respiratory epithelium (Figure 5I). By contrast, the ciliated cells of the respiratory epithelium exhibited barely detectable *LacZ* signals. In the epithelium of the alveoli in the lung, *LacZ* expression was dominantly observed in type II pneumocytes that secrete a surfactant and reduce surface tension within the alveoli, whereas almost no expression was detected in type I pneumocytes (data not shown). In the alveolar section, macrophage-like cells also exhibited *LacZ* expression (data not shown).

The epididymis is an extremely convoluted long duct extending down the posterior aspect of the testis to the lower pole where it becomes the spermiduct (Figure 3K). *LacZ* was expressed in the tall columnar cells of the pseudostratified epithelium lining the lumen of epididymis

Table 1. Tissue and cell type–specific expression of *LacZ-Rab27b*

Tissue/organ	Cell type	Functional category
Brain	Neuron subtype	Neuronal transmission
Spinal cord	Neuron subtype	
Ganglion	Neuron subtype	
Pituitary	Endocrine cells	Secretion
Thyroid glands	Endocrine cells	
Harderian glands	Exocrine cells	
Submandibular glands	Serous secretory cells/mucous secretory cells	
Pancreas	Exocrine cells/exocrine ducts cells	
Skin	Sebaceous secretory cells	
Stomach	Mucous-secreting cells/neck mucous cells	
	Acid-secreting parietal cells/enteroendocrine cells	
Small intestine	Goblet cells	
Large intestine	Goblet cells	
Trachea	Hyaline cartilage cells/Goblet cells	
Lung	Alveolar pneumocytes	
Eye ball	Corneal epithelial cells	Surface protection and mechanical extension
Skin	Stratified squamous epithelium (keratinocytes)	
Tongue	Stratified squamous epithelium	
Esophagus	Stratified squamous epithelium	
Heart	Coronary artery/atrium (valve)	
Liver	Endothelial cells (terminal branches of hepatic artery)	
Gall bladder	Mucosal epithelium	
Kidney	Transitional epithelium (renal pelvis)	
Ureter	Transitional epithelium	
Urinary bladder	Transitional epithelium (umbrella cells)	
Epididymis	Pseudostratified epithelium	
Spermiduct	Pseudostratified epithelium	
Uterus	Endometrium epithelium	
Spleen	Large nuclear cells (macrophages)	Phagocytosis and thrombopoiesis
Lymph node	Large nuclear cells	
Bone marrow	Megakaryocytes	

and spermiduct (Figure 5J). In the section of the spleen, we detected *LacZ* activity in extremely large-sized cells with huge irregular-shaped nuclei (Figure 5K). Their morphological characteristics suggest that they correspond to macrophages residing in the spleen. In the skin, a strong *LacZ* activity was detected in epidermal keratinocytes, whereas a weaker activity was observed in the sebaceous glands that secrete an oily substance onto the hair surface in the upper part of the hair follicle (Figure 5L). *LacZ* expression was also found in endothelial cells of the heart valve that show a leaflet structure supported by an elastic fibrous lamina beneath the endothelium (Figure 5M).

Table 1 presents the full list of tissues and cell types where *LacZ* was detected in the present study. We classified *LacZ*-expressing cell types into four functional categories: 1) neurons; 2) secretory cells in endocrine glands, exocrine glands, and the gastrointestinal tract; 3) epithelial or endothelial cells that are involved in surface protection and mechanical extension (the stratified squamous epithelium, transitional epithelium, and pseudostratified epithelium are three main elements); and 4) phagocytic and thrombopoietic cells.

Expression of Rab27 Isoforms in Pituitary Tissue

We previously reported that Rab27b is abundantly expressed in pituitary tissue, and especially in the pituitary corticotroph-derived cell line, AtT20, among the tissues and cells examined by immunoblot analysis (Zhao *et al.*, 2002). Here, we extended these findings by analyzing Rab27b expression in the pituitary in detail. The whole-mount *LacZ* staining of pituitary tissue from *Rab27b*$^{+/-}$ mice revealed strong activity, especially in the intermediate lobe, compared with the relatively weak activity in the anterior lobe (Figure 6A). Rab27b immunohistochemistry consistently detected abundant signals in the intermediate lobe of *Rab27b*$^{+/+}$ mice but not in that of *Rab27b*$^{-/-}$ mice. Conversely, immunohistochemistry with anti-β-galactosidase antibody showed positive signals in *Rab27b*$^{-/-}$ pituitary tissue but not in *Rab27b*$^{+/+}$ pituitary tissue.

We then compared the protein expression levels of Rab27a and Rab27b, because both isoforms are expressed in pituitary tissues (Yi *et al.*, 2002; Zhao *et al.*, 2002). An isolated pituitary was separated into anterior and intermediate-posterior lobes, and each tissue lysate was prepared separately. Using bacterially expressed recombinant proteins as standards, the amounts of endogenous proteins were analyzed by immunoblotting with anti-Rab27a and anti-Rab27b antibodies (Figure 6B), which specifically recognize the respective isoforms (Zhao *et al.*, 2002). We estimated that Rab27a and Rab27b constituted ~0.1% and ~0.0005% in the anterior pituitary and ~0.2% and ~0.05% in the intermediate-posterior pituitary, respectively, of the total protein extracts (Figure 6C). These values roughly agree with the previous estimations for the Rab27a and Rab27b protein levels in the total pituitary tissue (Chen *et al.*, 2003).

Electron Microscopic Analysis of Secretory Granule Distribution

Because both Rab27a and Rab27b are expressed in the anterior pituitary (Figure 6, B and C) and likely play a complementary role in coexpressed cells (Barral *et al.*, 2002), we generated *Rab27a*$^{ash/ash}$*Rab27b*$^{-/-}$ double mutant mice by crossing Rab27b knockout mice with Rab27a-deficient *ashen*

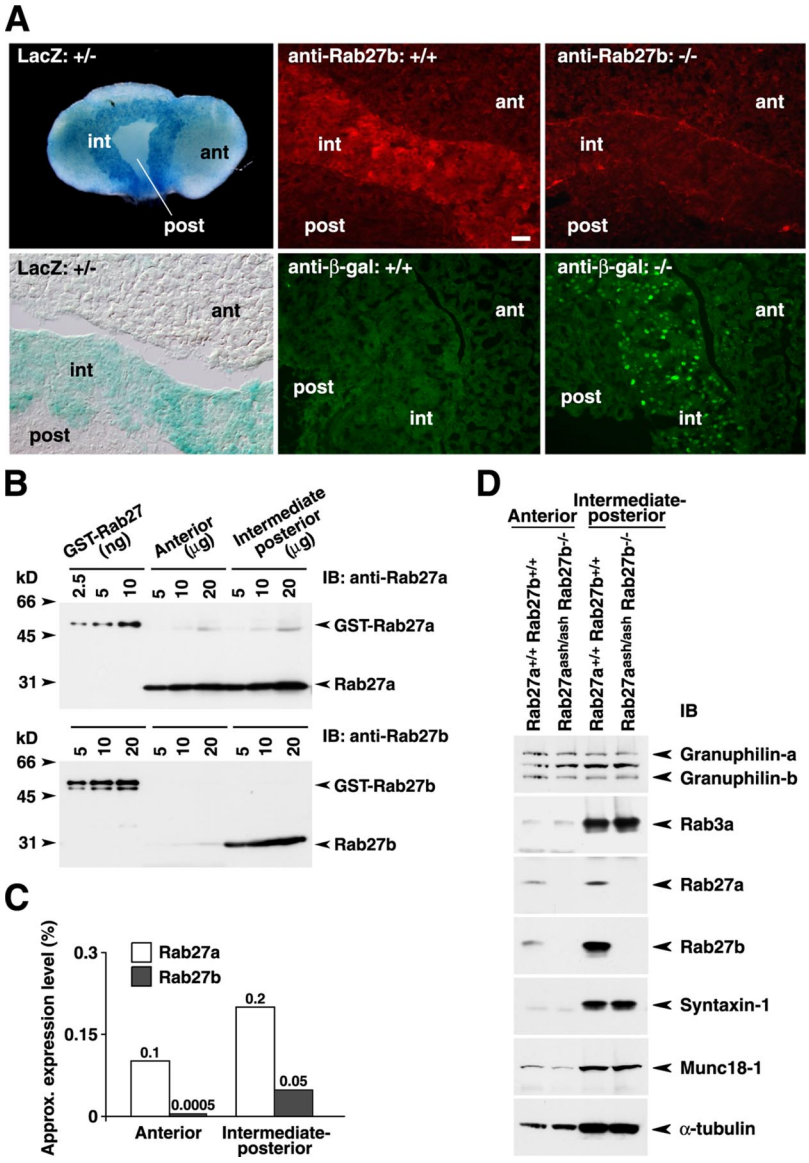

Figure 6. Expression of Rab27b and Rab27a in the pituitary. (A) Whole-mount *LacZ* staining of the pituitary from *Rab27b*$^{+/-}$ mice (left panels). Immunohistochemistry with either anti-Rab27b or anti-β-galactosidase antibody in *Rab27b*$^{+/+}$ pituitary (center panels) and *Rab27b*$^{-/-}$ pituitary tissues (right panels). ant, anterior lobe; int, intermediate lobe; and post, posterior lobe. Bar, 20 μm. (B) The amounts of Rab27a and Rab27b in lysates of anterior and intermediate-posterior pituitary were determined by immunoblotting with isoform-specific antibodies, using known amounts of GST-Rab27a and GST-Rab27b proteins as standards. (C) The expression levels of endogenous Rab27a and Rab27b in each lobe, which were estimated from the intensities of the immunoblot signals, are shown as a percentage of the total extracted proteins. (D) Thirty micrograms of proteins from the anterior or intermediate-posterior pituitary from *Rab27a*$^{ash/ash}$*Rab27b*$^{-/-}$ double mutant mice were electrophoresed and immunoblotted with the indicated antibodies.

mice. The double mutant mice were viable and showed no gross abnormalities in development or behavior, except for the diluted coat color and minor defects in reproduction characteristic of *ashen* mice. We confirmed that neither Rab27a nor Rab27b was expressed in the anterior or intermediate-posterior pituitary of the double mutant mice (Figure 6D). The expression levels of other exocytic proteins, including that of the Rab27 effector, granuphilin, was not changed.

We previously showed that Rab27a and granuphilin play critical roles in the docking and recruitment of insulin granules to the plasma membrane in pancreatic β-cells (Gomi *et al.*, 2005; Kasai *et al.*, 2005). Thus, we next examined the intracellular distribution of secretory granules in the pituitary by electron microscopy. Corticotrophs harbor electron-dense ACTH granules and can be easily discriminated by their stellate or U/ring-shaped morphology with cytoplasmic processes embracing growth hormone (GH)-containing somatotrophs (Siperstein and Miller, 1970). The top panels of Figure 7A show the representative electron micrographs of U-shaped corticotrophs with two long cytoplasmic processes. In wild-type corticotrophs, the ACTH granules tended to be distributed in a row along the plasma membrane and accumulated at the distal portion of the processes. However, in *Rab27a*$^{ash/ash}$*Rab27b*$^{-/-}$ double mutant corticotrophs, such polarized distribution in the cell periphery was markedly disturbed and more ACTH granules resided in the cell interior and at the proximal region of the processes. The morphometric analysis measuring the distance between the granule center and the nearest plasma membrane clearly demonstrated a decrease in the number of granules in the periphery and an increase in that in the interior of the double mutant cells (Figure 7B). However, such changes were much milder in either *Rab27b*$^{-/-}$ or *Rab27a*$^{ash/ash}$ single mutant cells (Figure 7B), suggesting that the presence of the other isoform partially compensated for the defect.

We also examined the distribution of ACTH granules in mice devoid of granuphilin (Gomi *et al.*, 2005), which is normally expressed in corticotrophs (Zhao *et al.*, 2002). The polarized peripheral distribution of ACTH granules was more strongly impaired in granuphilin-null cells than in the Rab27a/Rab27b double mutant cells, although both strains

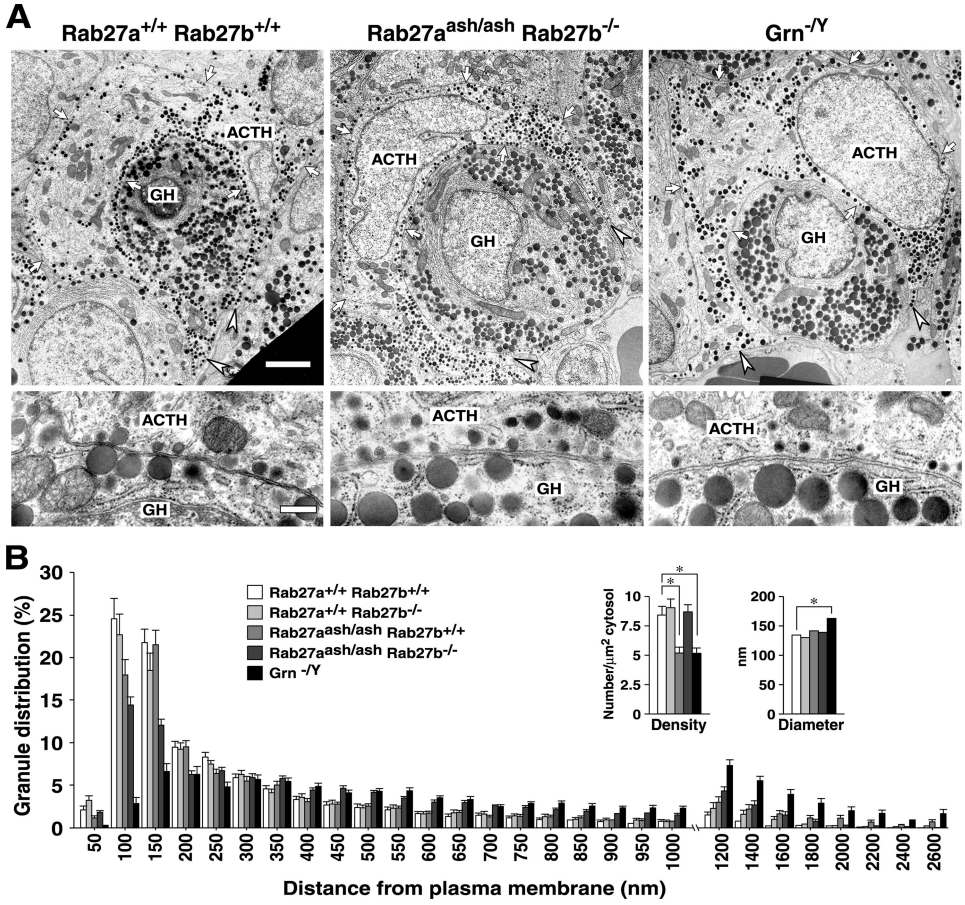

Figure 7. Electron microscopic analysis of the anterior pituitary. (A) Electron micrographs of anterior pituitary sections from 7-mo-old male control *Rab27a*$^{+/+}$*Rab27b*$^{+/+}$ (left), *Rab27a*$^{ash/ash}$*Rab27b*$^{-/-}$ double mutant (center), and granuphilin-null mutant (*Grn*$^{-/Y}$) mice (right). Top panels, the typical cell arrangement of ACTH-containing corticotrophs with long processes surrounding GH-containing somatotrophs. Arrows indicate the boundary of corticotrophs, whereas arrowheads show the tip of the process. Bar, 2 μm. Bottom, at a higher magnification, ACTH and GH granules located close to the plasma membrane in adjacent corticotrophs and somatotrophs. Bar, 200 nm. (B) Morphometry of ACTH granule distribution, density, and diameter in corticotrophs. All granules located in the single section were categorized according to the distance between their center and the plasma membrane. The data are represented as a percentage of the granule number in 20 cells each from *Rab27a*$^{+/+}$*Rab27b*$^{+/+}$, *Rab27a*$^{+/+}$*Rab27b*$^{-/-}$, *Rab27a*$^{ash/ash}$*Rab27b*$^{+/+}$, and *Rab27a*$^{ash/ash}$*Rab27b*$^{-/-}$ mice, and 21 cells from *Grn*$^{-/Y}$ mice. For each group, pituitary tissues were analyzed from two different animals. Granule density was calculated from the granule number per cytosol area (μm^2). Granule diameter (nm) was calculated from 527 granules in each genotype. Results are presented as the mean ± SEM. *$p < 0.001$; ANOVA, Scheffe's posthoc test.

have the same genetic background: C3H/He (Figure 7, A and B). Interestingly, those docked granules whose limiting membrane directly attached to the plasma membrane were deficient in granuphilin-null corticotrophs, whereas they were only modestly decreased in Rab27a/Rab27b double mutant cells (Figure 7A). Furthermore, the docking of GH-containing granules in adjacent somatotrophs, which also express granuphilin (Zhao *et al.,* 2002), was similarly impaired specifically in granuphilin-null cells (Figure 7A). Because the diameter of the ACTH granules was 130~160 nm (Figure 7B), granules whose center resided within 100 nm of the plasma membrane should include almost all the docked granules. Indeed, the number of such granules was dramatically reduced in granuphilin-null corticotrophs, even compared with Rab27a/Rab27b double mutant cells (Figure 7B). The difference in the docking state between these two mutants is consistent with the previous electron microscopic findings that the number of docked insulin granules was drastically reduced in granuphilin-null pancreatic β-cells but not significantly so in *ashen* β-cells (Gomi *et al.,* 2005; Kasai *et al.,* 2005). Slight changes in the granule density and in the granule diameter detected in granuphilin-null corticotrophs (Figure 7B) have also been found in granuphilin-null β-cells (Gomi *et al.,* 2005).

ACTH Secretion from the Pituitary

We previously reported that overexpression of inactive Rab27b mutant protein dominant-negatively inhibits ACTH secretion in cultured AtT20 cells (Zhao *et al.,* 2002). To examine whether loss of the Rab27 isoform affects ACTH secretion, we performed perifusion analyses in pituitary tissues of *Rab27a*$^{ash/ash}$*Rab27b*$^{-/-}$ mice. The anterior pituitary was exposed to a physiological secretagogue, CRF, and then to a high KCl concentration. The control anterior pituitary showed a gradual but significant increase of ACTH secretion in response to CRF and a steep and large increase in response to the depolarization stimulus (Figure 8A). ACTH secretion from the double mutant pituitary was not significantly changed, although it showed a slight decrease in response to each of the two stimuli. Thus, the complete loss of Rab27 proteins in corticotrophs causes only modest, if any, impairment in evoked ACTH secretion. By contrast, evoked ACTH secretion was increased in granuphilin-null pituitary tissue compared with wild-type pituitary tissue (Figure 8B). This finding is again consistent with the previous finding that evoked insulin secretion is increased despite the severe reduction in docked granules in granuphilin-null pancreatic β-cells (Gomi *et al.,* 2005).

DISCUSSION

We here report findings obtained from a newly constructed knockin mouse model that lacks Rab27b and instead expresses *LacZ* under the control of the authentic Rab27b promoter. X-gal staining of the tissues in heterozygous mice indicates the cell types that endogenously express Rab27b protein. This kind of knockin mouse is particularly useful for examining gene expression in minor cell types such as

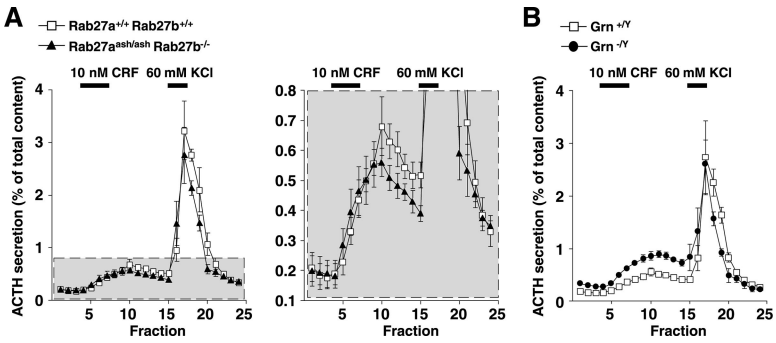

Figure 8. ACTH secretion profiles in perifused pituitary tissue. (A) The anterior lobe was stimulated first with 10 nM CRF for 15 min and then with 60 mM KCl for 10 min (horizontal black lines). The perifusate was fractionated every 4 min into a 2-ml aliquot. Relative ACTH secretion (% of total content) is shown for 9-mo-old male *Rab27a*$^{+/+}$*Rab27b*$^{+/+}$ control (□) and *Rab27a*$^{ash/ash}$-*Rab27b*$^{-/-}$ double mutant (▲) mice (n = 4). The gray area enclosed with a dotted line (left panel) is expanded to make the differences clearer (right panel). Results are presented as the mean ± SEM. (B) ACTH secretion profiles were examined as in A for 9-mo-old male wild-type (*Grn*$^{+/Y}$, □) and granuphilin-null (*Grn*$^{-/Y}$, ●) mice (n = 4).

secretory cells, which may elude detection by analysis at the whole tissue level, as in the case of immunoblotting. Furthermore, unlike conventional immunostaining studies, this model avoids the need for an antibody with high-affinity and specificity and is not affected by artifacts due to histochemical treatment. Recently, the expression of Rab27a has been examined using a PAC-based transgenic mouse that expresses an EGFP-Rab27a fusion protein under the control of the Rab27a endogenous promoter (Tolmachova *et al.*, 2004). Although this approach yields useful data, we cannot exclude the possibility that the transgene expression is influenced at the position inserted in a chromosome. Furthermore, the autofluorescence intrinsic in tissues elicited by light excitation could obscure detection or specificity of the EGFP signals. For these reasons, the sort of reporter knockin mouse adopted here is well suited for determining the cell types that express any gene product.

The comprehensive analysis of the Rab27b expression indicates noticeable differences in the expression patterns between Rab27a and Rab27b, although Rab27b is also expressed in a broad range of specialized secretory cells. First, Rab27b is expressed in neurons in particular brain regions, whereas Rab27a is not detectable in brain tissue by a conventional immunoblot analysis (Yi *et al.*, 2002), although some neuroendocrine neurons express Rab27a (Gomi and Izumi, unpublished data). Second, Rab27b is expressed in distinct types of secretory cells compared with those expressing Rab27a. In the pituitary, for example, Rab27b is most preferentially expressed in the intermediate lobe, whereas Rab27a is expressed in both the anterior and intermediate-posterior lobes. Further, Rab27b is highly expressed in pancreatic exocrine cells but not in islet cells. Conversely, Rab27a is easily detected in islets cells but not in acinar cells by immunostaining analysis (Yi *et al.*, 2002; Yu *et al.*, 2007), although the EGFP-Rab27a fusion protein is detected in the acinar cells of the transgenic mouse model (Tolmachova *et al.*, 2004). Third, Rab27b is widely expressed in the cells that are engaged in surface protection and mechanical extension. In addition to its expression in the transitional epithelium of umbrella cells, as was previously reported (Chen *et al.*, 2003), it is expressed in the stratified squamous epithelium of the skin and esophagus, the pseudostratified epithelium of the epididymis, and the endothelial cells of heart valves. Rab27a has not been reported to be expressed in these cells. In summary, Rab27b is expressed not only in classical secretory cells but also in more broadly defined exocytic cells, such as those providing surface membrane in response to mechanical stress.

At the whole body level, Rab27b-null mice exhibited no gross abnormalities in development, behavior, or reproduction. This may explain why human disease or animal mutants with Rab27b gene mutations have not been discovered previously. The Rab27a/Rab27b double mutant mice also showed apparently normal phenotypes, except for the diluted coat color and minor reproductive defects that single Rab27a-null *ashen* mice exhibit. These findings are consistent with a recent report about independently manufactured Rab27b-null and Rab27a/Rab27b double mutant mice (Tolmachova *et al.*, 2007). However, detailed specific tests would likely uncover dysfunction of various cell types in these mutant mice. In fact, it has been shown that Rab27a and Rab27b play both redundant and distinct roles in the regulation of the number and secretion of platelet dense granules (Tolmachova *et al.*, 2007). We also detected morphological changes in some cell types in the Rab27b knockout mice (Gomi and Izumi, unpublished observations). Given that the expression of Rab27a (Tolmachova *et al.*, 2004) and of Rab27b (per the present findings) are thoroughly disclosed, the next step is to examine the common and distinct functions of Rab27a and Rab27b in each cell type. The Rab27b single and Rab27a/Rab27b double knockout mice generated in the present study should certainly become valuable tools for this purpose.

We showed that ACTH secretion from anterior pituitary was only minimally affected in the Rab27a/Rab27b double mutant mice, although more sensitive assays might reveal some aspects of secretion defects. We previously reported that Rab27a deficiency decreases insulin secretion only in response to a high glucose concentration but not to a high KCl concentration in pancreatic β-cells, where Rab27b is not normally expressed (Kasai *et al.*, 2005). These findings collectively indicate that the Rab27 subfamily does not play an essential role in the release of secretory granules, in contrast to the crucial role of Rab27a in the exocytosis of lytic granules in cytotoxic T lymphocytes (Ménasché *et al.*, 2000; Haddad *et al.*, 2001; Stinchcombe *et al.*, 2001). The Rab27 subfamily and its effector, granuphilin, however, play decisive roles in the intracellular distribution of secretory granules. We demonstrated that the polarized localization of granules to the cell periphery is markedly affected in Rab27a/Rab27b double mutant corticotrophs. Moreover, granuphilin-deficient cells exhibit more pronounced disturbance in the peripheral localization of granules, with almost complete loss of docked granules. Therefore, both Rab27a/Rab27b and granuphilin are essential for the delivery of granules close to the plasma membrane, and granuphilin is further required for the fixation of granule-docking to the plasma membrane. These findings are consistent with our previous electron microscopic findings for insulin granules in equivalent mutant pancreatic β-cells (Gomi *et al.*, 2005; Kasai *et al.*, 2005). The quantitative and qualitative differences in granule localization between Rab27a/Rab27b double mutant and granuphilin mutant cells indicate distinct and overlapping regulatory roles for these molecules. In the

final docking process, Rab27 proteins might have only a regulatory role, whereas granuphilin has a physical role. Alternatively, the existence of related Rab proteins, such as Rab3, and/or other coexpressed Rab27 effectors might modify the phenotypes of these mutant cells. In any case, it should be noted that neither mutant exhibits a significant decrease in evoked ACTH secretion despite the reduction in granules located close to the plasma membrane. Thus, the degree of the morphological docking to the plasma membrane, or even that of the peripheral localization, cannot predict the number of releasable granules in response to secretagogues. Although it is widely believed that the stably docked vesicles constitute a readily releasable pool, the present findings and the previous finding in granuphilin-null pancreatic β-cells (Gomi *et al.*, 2005) strongly indicate that the stable predocking of vesicles to the exocytic site is not necessarily required for subsequent release. Thus, we must investigate the possible existence of unidentified mechanisms that allow granules located in relatively remote areas from the plasma membrane to translocate and fuse efficiently.

ACKNOWLEDGMENTS

We thank Drs. T. Yagi and K. Yamamura for the DNAs to construct the targeting vector. We are also grateful for technical assistance from T. Ishizaka, E. Sone, and K. Fuse for the morphometric analyses; T. Nara and S. Kanai for the mouse colony maintenance; and Y. Onodera, A. Okada, Y. Saito, and H. Suzuki for the ES cell injection. This work was supported by grants-in-aids for scientific research and Global Center of Excellence Program from the Ministry of Education, Culture, Sports, Science, and Technology of Japan, and in part by grants from Novo Nordisk Insulin Study Award and Astellas Foundation for Research on Metabolic Disorders (T. I.).

REFERENCES

Bahadoran, P., Aberdam, E., Mantoux, F., Buscà, R., Bille, K., Yalman, N., de Saint-Basile, G., Casaroli-Marano, R., Ortonne, J.-P., and Ballotti, R. (2001). Rab27a: a key to melanosome transport in human melanocytes. J. Cell Biol. *152*, 843–849.

Barral, D. C., Ramalho, J. S., Anders, R., Hume, A. N., Knapton, H. J., Tolmachova, T., Collinson, L. M., Goulding, D., Authi, K. S., and Seabra, M. C. (2002). Functional redundancy of Rab27 proteins and the pathogenesis of Griscelli syndrome. J. Clin. Invest. *110*, 247–257.

Chen, X., Li, C., Izumi, T., Ernst, S. A., Andrews, P. C., and Williams, J. A. (2004). Rab27b localizes to zymogen granules and regulates pancreatic acinar exocytosis. Biochem. Biophys. Res. Commun. *323*, 1157–1162.

Chen, Y., Guo, X., Deng, F.-M., Liang, F.-X., Sun, W., Ren, M., Izumi, T., Sabatini, D. D., Sun, T.-T., and Kreibich, G. (2003). Rab27b is associated with fusiform vesicles and may be involved in targeting uroplakins to urothelial apical membranes. Proc. Natl. Acad. Sci. USA *100*, 14012–14017.

Fukuda, M. (2005). Versatile role of Rab27 in membrane trafficking: focus on the Rab27 effector families. J. Biochem. *137*, 9–16.

Gomi, H., Mizutani, S., Kasai, K., Itohara, S., and Izumi, T. (2005). Granuphilin molecularly docks insulin granules to the fusion machinery. J. Cell Biol. *171*, 99–109.

Gomi, H., Yokoyama, T., Fujimoto, K., Ikeda, T., Katoh, A., Itoh, T., and Itohara, S. (1995). Mice devoid of the glial fibrillary acidic protein develop normally and are susceptible to scrapie prions. Neuron *14*, 29–41.

Grosshans, B. L., Ortiz, D., and Novick, P. (2006). Rabs and their effectors: achieving specificity in membrane traffic. Proc. Natl. Acad. Sci. USA *103*, 11821–11827.

Haddad, E. K., Wu, X., Hammer, J. A., 3rd, and Henkart, P. A. (2001). Defective granule exocytosis in Rab27a-deficient lymphocytes from *Ashen* mice. J. Cell Biol. *152*, 835–841.

Hume, A. N., Collinson, L. M., Repak, A., Gomes, A. Q., Hopkins, C. R., and Seabra, M. C. (2001). Rab27a regulates the peripheral distribution of melanosomes in melanocytes. J. Cell Biol. *152*, 795–808.

Imai, A., Yoshie, S., Nashida, T., Shimomura, H., and Fukuda, M. (2004). The small GTPase Rab27B regulates amylase release from rat parotid acinar cells. J. Cell Sci. *117*, 1945–1953.

Izumi, T., Gomi, H., Kasai, K., Mizutani, S., and Torii, S. (2003). The roles of Rab27 and its effectors in the regulated secretory pathways. Cell Struct. Funct. *28*, 465–474.

Kasai, K., Ohara-Imaizumi, M., Takahashi, N., Mizutani, S., Zhao, S., Kikuta, T., Kasai, H., Nagamatsu, S., Gomi, H., and Izumi, T. (2005). Rab27a mediates the tight docking of insulin granules onto the plasma membrane during glucose stimulation. J. Clin. Invest. *115*, 388–396.

Ménasché, G. *et al.* (2000). Mutations in *RAB27A* cause Griscelli syndrome associated with haemophagocytic syndrome. Nat. Genet. *25*, 173–176.

Ramalho, J. S., Tolmachova, T., Hume, A. N., McGuigan, A., Gregory-Evans, C. Y., Huxley, C., and Seabra, M. C. (2001). Chromosomal mapping, gene structure and characterization of the human and murine RAB27B gene. BMC Genet. *2*, 2.

Siperstein, E. R., and Miller, K. J. (1970). Further cytophysiologic evidence for the dentity of the cells that produce adrenocorticotrophic hormone. Endocrinology *86*, 451–486.

Stinchcombe, J. C., Barral, D. C., Mules, E. H., Booth, S., Hume, A. N., Machesky, L. M., Seabra, M. C., and Griffiths, G. M. (2001). Rab27A is required for regulated secretion in cytotoxic T lymphocytes. J. Cell Biol. *152*, 825–833.

Tiwari, S., Italiano, J. E., Jr., Barral, D. C., Mules, E. H., Novak, E. K., Swank, R. T., Seabra, M. C., and Shivdasani, R. A. (2003). A role for Rab27b in NF-E2-dependent pathways of platelet formation. Blood *102*, 3970–3979.

Tolmachova, T., Åbrink, M., Futter, C. E., Authi, K. S., and Seabra, M. C. (2007). Rab27b regulates number and secretion of platelet dense granules. Proc. Natl. Acad. Sci. USA *104*, 5872–5877.

Tolmachova, T., Anders, R., Stinchcombe, J., Bossi, G., Griffiths, G. M., Huxley, C., and Seabra, M. C. (2004). A general role for Rab27a in secretory cells. Mol. Biol. Cell *15*, 332–344.

Wilson, S. M., Yip, R., Swing, D. A., O'Sullivan, T. N., Zhang, Y., Novak, E. K., Swank, R. T., Russell, L. B., Copeland, N. G., and Jenkins, N. A. (2000). A mutation in *Rab27A* causes the vesicle transport defects observed in *ashen* mice. Proc. Natl. Acad. Sci. USA *97*, 7933–7938.

Yanagawa, Y., Kobayashi, T., Ohnishi, M., Kobayashi, T., Tamura, S., Tsuzuki, T., Sanbo, M., Yagi, T., Tashiro, F., and Miyazaki, J. (1999). Enrichment and efficient screening of ES cells containing a targeted mutation: the use of DT-A gene with the polyadenylation signal as a negative selection marker. Transgenic Res. *8*, 215–221.

Yi, Z., Yokota, H., Torii, S., Aoki, T., Hosaka, M., Zhao, S., Takata, K., Takeuchi, T., and Izumi, T. (2002). The Rab27a/granuphilin complex regulates the exocytosis of insulin-containing dense-core granules. Mol. Cell. Biol. *22*, 1858–1867.

Yu, M., Kasai, K., Nagashima, K., Torii, S., Yokota-Hashimoto, H., Okamoto, K., Takeuchi, T., Gomi, H., and Izumi, T. (2007). Exophilin4/Slp2-a targets glucagon granules to the plasma membrane through unique Ca^{2+}-inhibitory phospholipid-binding activity of the C2A domain. Mol. Biol. Cell *18*, 688–696.

Zhao, S., Torii, S., Yokota-Hashimoto, H., Takeuchi, T., and Izumi, T. (2002). Involvement of Rab27b in the regulated secretion of pituitary hormones. Endocrinology *143*, 1817–1824.